Chemical Engineering Journal 432 (2022) 134427

Contents lists available at ScienceDirect

Chemical Engineering Journal

journal homepage: www.elsevier.com/locate/cej

Contribution of thermal expansion on gas adsorption to coal sorption-induced swelling

Junqiang Kang [a,b], Derek Elsworth [b], Xuehai Fu [a,*], Shun Liang [c], Hao Chen [d]

[a] Key Laboratory of Coalbed Methane Resources and Reservoir Formation Process, Ministry of Education, China University of Mining and Technology, Xuzhou, Jiangsu 221008, China
[b] Energy and Mineral Engineering, G3 Center and EMS Energy Institute, Pennsylvania State University, University Park, PA, USA
[c] School of Mines, Key Laboratory of Deep Coal Resource Mining, Ministry of Education of China, China University of Mining and Technology, Xuzhou, China
[d] PetroChina Research Institute of Petroleum Exploration and Development, Beijing 100083, China

ARTICLE INFO

Keywords:
Gas adsorption
Adsorption heat
Thermal expansion
Sorption-induced swelling

ABSTRACT

Adsorption of gases such as methane and carbon dioxide in coal is an exothermic process. Under isentropic conditions (fully insulated condition), the ejected heat results in an additive transient thermal expansion in addition to the sorption-induced swelling. The magnitude of thermal expansion and its feedback on methane adsorption remains ill-defined. We explore this response in high volatile bituminous coal by measuring the exothermal release of heat (integral heat of adsorption) via temperature change during methane adsorption and use these calorimetric data to define the thermodynamic response. These data link thermal expansion directly to adsorption and adsorption swelling. The results show that methane adsorption can lead to the elevation of coal temperature by more than 10 °C. The resulting thermal expansion is consistent with adsorption swelling and related to adsorption capacity and pressure. The decline of surface potential energy resulting from adsorption is usually considered to be the reason for adsorption swelling. However, the results of this study show that thermal expansion due to the heat of adsorption may account for up to 35% of the total adsorption strain under ideal isentropic conditions. In non-isentropic laboratory experiments of adsorption swelling (approaching isothermal conditions), thermal expansion during adsorption cannot be measured accurately due to the rapid heat loss. However, in-situ within coalbed reservoirs, reduced heat dissipation may retain thermal deformation for longer and impact short-term permeability evolution.

1. Introduction

Methane desorption and carbon dioxide adsorptions are the most important parts of coalbed methane (CBM) production and carbon dioxide geological storage (CGS), respectively, which will results in coal matrix shrinkage or swelling and impact permeability [1–3]. Adsorption and desorption are exothermic and endothermic processes respectively, which can also cause drive a decline in reservoir temperature [4–9] with secondary feedback in further impacting permeability and related CBM production/CGS.

Gas desorption involves the transformation of the gas from an adsorbed to a free state. This transformation absorbs heat from the reservoir to elevate the molecular kinetic energy of the gas as it is released into a free state and causing a decline in reservoir temperature [4–9]. Adsorption is the reverse process - resulting in a rise in reservoir temperature. The heat released as a result of gas adsorption is usually expressed as a differential heat of adsorption (Q_{st}) and integral adsorption heat (Q) [10]. The Q_{st} is the heat released per unit mass of adsorbate absorbed on the adsorbent and is equivalent to the change in enthalpy (ΔH). Q refers to the heat released as the adsorbate adsorbs to a unit mass of adsorbent and is equivalent to the product of Q_{st} and adsorbed mass. This exothermic response coals of different metamorphic states show that Q_{st} is of the order 20–60 kJ/mol and greater for CO_2 than methane [11]. The variation of Q_{st} with time/mass is similar to Langmuir adsorption [4] with the Q of methane adsorption between 11.22 and 25.14 J/g and increasing with an increase in the degree of coal metamorphism [12]. If the system is isentropic then the temperature change may be more than 10 °C at saturation with the temperature increment

* Corresponding author at: Postal Address:Room 345 of Key Laboratory of Coalbed Methane Resources and Reservoir Formation Process, China University of Mining and Technology, Jinshan East Road, Xuzhou, Jiangsu Province 221000, China.
E-mail address: fuxuehai@cumt.edu.cn (X. Fu).

https://doi.org/10.1016/j.cej.2021.134427
Received 28 October 2021; Received in revised form 25 December 2021; Accepted 28 December 2021
Available online 31 December 2021

proportional to the adsorbed mass [4,11,13]. The results of Guo (2000) [4] show that CO_2 can increase the coal temperature by 10 °C in 0.46 MPa adsorption pressure, and the temperature increment with adsorption time shows a Langmuir adsorption curve. Liu (2014) [14] used an infrared camera to detect the temperature change during the methane desorption of medium-rank coal. The results showed that after coal was saturated with 2 MPa methane, the sample temperature decreased by 2–4 °C in desorption [14]. With the decreasing particle size, the greater the temperature decrease [14]. Liu (2015) [15] studied the temperature changes on the coal surface in methane adsorption of 1.6 MPa and desorption of 1.56 MPa of anthracite, and found that the temperature increases by more than 5 °C and the maximum exceeds 8 °C in adsorption; while the temperature also decreases by 4 °C and the maximum exceeds 7 °C in desorption [15]. The temperature change gradually decreases with the increase of time, because the adsorption/desorption rate decreases and the endothermic/exothermic rate is less than the heat loss [15]. Yue (2015) [10] studied the temperature change during the methane adsorption of 2 MPa in pulverized anthracite particles, and found that the temperature of the coal sample caused by adsorption heat could be as high as 13.79 °C. Zhou (2017) [6] used thermography to study the temperature change of anthracite in methane adsorption, and the results based on theoretical analysis show that the temperature could be increased by 2–20 °C after coal adsorption saturation. Feng (2017) directly measured the temperature change of the anthracite surface during methane adsorption and found that under the adsorption pressure of 1.2 MPa, the temperature after 10 s exceeded 2 °C [7]. Zhao (2018) used infrared observation to directly observe the surface temperature changes of anthracite and bituminous coal samples during methane adsorption at 0.3 MPa, and found that the surface temperature of coal samples increased significantly with time [16]. The results of Li (2018) [17] for anthracite also showed that the coal temperature increased at 20 ℃ when the coal adsorption saturation. Since the increment in temperature is proportional to adsorbed mass the temperature shows a Langmuir-type relation [12].

The current research shows that there are obvious temperature changes in the adsorption process, and the research is in the low-pressure stage, and the maximum adsorption pressure does not exceed 2 MPa [4–7,14–16], which is far from reaching saturated adsorption, which means that if the adsorption pressure is increased, the temperature will continue to rise. Moreover, it can be seen that the change of coal surface temperature measured by infrared measurement is small [7,14,16], because the coal surface temperature dissipates rapidly. But the internal adsorption study of pulverized coal through temperature sensor shows that the temperature increases significantly under the same adsorption pressure [10], because the heat loss is slow in coal inside and the temperature will rise higher. The results of Fan (2019) [8] show the temperature of the coal reservoir increases by 18 °C when CO_2 is injected into in-situ coal reservoir, which is significantly higher than that of laboratory measurement. The temperature change during gas desorption is used as the prediction index of gas outburst [9,18–19].

The thermal expansion coefficient is very important for the temperature change to affect deformation. Bangham and Franklin (1946) [20] measured that the thermal expansion coefficient of coal at 20-100 °C was 0.0032%/K to 0.0039%/K. MacRae and Ryder (1955) [21] measured that the thermal expansion coefficient of bright coal at 0-20 °C was 0.0031% to 0.0059%/K. Zhu (2011) [22] measured that the volumetric thermal expansion coefficient of coal was 0.0042%/K. Feng (2017) measured that the thermal expansion coefficient of anthracite at 0–100 °C is about 0.0020%/K [7]. It assumes that the adsorption pressure has a temperature change of 5 °C at 3 MPa, and the thermal deformation is 0.0030%/K, so the thermal deformation is 0.015%. This strain can not be ignored in most adsorption deformation strain measurements [23–25]. Thermal deformation eventually leads to the decline of reservoir permeability [26–27]. Under the constant effective stress, permeability decreases linearly with increasing temperature [28] and at 55 °C may decrease by ~50% relative to that at 30 °C. Observations show that permeability generally decreases with an increase in temperature and increases with a reduction in temperature [29]. Thus, the expansion that results from an increase in temperature can significantly affect reservoir permeability but thermal effects are typically ignored [30–32]. We target the transient contribution of thermal expansion to overall adsorption swelling as a result of adsorption in the following.

To study the general law of thermal expansion in the adsorption process, taking methane adsorption as an example, we measure the integral adsorption heat of gas adsorption and compare these results with those calculated based on thermodynamic theory (using isothermal adsorption experiments at different temperatures). This constrains thermodynamic response. We also measure thermal expansion resulting from adsorption-induced temperature change. By comparing with the previous P&C adsorption swelling theory based on surface potential energy change [32], the contribution of thermal expansion to adsorption swelling is defined. This provides the necessary theoretical background for a comprehensive understanding of adsorption swelling.

2. Review of theoretical models of adsorption swelling

The viability of CBM production and CGS from low permeability coal reservoirs relies on the ability to permeability change. Thus, a variety of mathematical models have been established to interpret and predict permeability evolution as controlled by stress, pressure, sorption, and structure [33]. One key parameter in these models is the nature of the swelling strain caused by gas adsorption. Current models universally adopt adsorption swelling strain controlled by a Langmuir isotherm [33], based on empirical data rather than a strict theoretical derivation [34]. To establish an improved model that accommodates the true response of non-isothermal sorption, it is necessary to understand the fundamental mechanics of adsorption and related volume changes.

Swelling is caused by a decrease in surface chemical potential energy and a decrease in the surface tension in adsorption [35–37]. The decrease in surface tension results in coal swelling with a linear relationship between swelling strain and change in chemical potential energy, as,

$$\varepsilon = \theta \Delta\gamma \tag{1}$$

where ε is the linear swelling strain (directional swelling not volumetric); θ is a constant related to Young's modulus and density of the adsorbent, and $\Delta\gamma$ is the change in chemical potential energy.

Subsequently, Yates (1954) established an adsorption swelling model based on a spherical model hypothesis based on the change in chemical potential energy [30]:

$$\Delta V = 2/3K\Delta\gamma \tag{2}$$

where ΔV is volumetric expansion strain; and K is the bulk modulus. The difference between the fundamental relations of Bangham (1930, 1934, 1946) [35–37] and Yates (1954) [30] and measurement prompted the hypothesis that adsorption results in a decrease in surface potential energy promotion, swelling, and increase in surface area of the adsorbate [31]. The capillary force produced by swelling is equal to the change in surface chemical potential energy. Based on a spherical porous medium, the adsorption swelling strain may be defined as:

$$\varepsilon = -(\Delta\gamma S\rho_s/E_s)f(x, v_s) \tag{3}$$

where $f(x,v_s)$ is:

$$f(x, v_s) = \frac{[2(1-v_s)-(1+v_s)cx][3-5v_s-4(1-2v_s)cx]}{(3-5v_s)(2-3cx)} \tag{4}$$

The Young's modulus and Poisson's ratio of the skeleton may be obtained as:

$$\begin{cases} E = \dfrac{E_s\rho}{3\rho_s - 2\rho} \\ v = v_s + \dfrac{3(1-v_s^2)(1-5v_s)\phi}{2(7-5v_s)} \end{cases} \tag{5}$$

where S is specific surface area, m^2/g; E is Young's modulus, Pa; E_s is the skeletal Young's modulus, Pa; ρ is apparent density, kg/m^3; ρ_s is skeleton density, kg/m^3; v is Poisson's ratio; v_s is skeletal Poisson's ratio; c is conversion coefficient of three vertical intersecting fractures, estimated as 1.2, and $\times$ is the ratio of matrix width to fracture width, estimated as 0.0005 [32].

Pan and Connell (2007) introduced the deformation model of Scherer (1986) into the study of swelling of methane and carbon dioxide adsorbed coal [32]. Based on the thermodynamics of adsorption, the change of surface chemical potential energy caused by adsorption is:

$$\Delta\gamma = \int_0^P V^a dP - RT\int_0^P \left(\sum_{i=1}^{C} n_i^a d\ln f_i\right) \tag{6}$$

Combined with Eq. (4) and the Langmuir isotherm, swelling strain within coal is defined as:

$$\varepsilon = RTV_L ln\left(1+\frac{p}{p_L}\right)\frac{\rho_s}{E_s}f(x,v_s) - \frac{p}{E_s}(1-2v_s) - \frac{3f(x,v_s)}{(1-\phi)E_s}\int_0^p \varepsilon dp \tag{7}$$

At low gas pressure, this may be simplified to:

$$\varepsilon = RTV_L ln\left(1+\frac{p}{p_L}\right)\frac{\rho_s}{E_s}f(x,v_s) - \frac{p}{E_s}(1-2v_s) \tag{8}$$

where p is gas pressure, Pa; V^a is the adsorption volume, mol/kg; R is the ideal gas constant; T is the temperature of the isothermal adsorption experiment, K; n_i^a is adsorption capacity under unit pressure change; f is fugacity, effective pressure of the gas, Pa; V_L is the Langmuir volume, mol/kg; and p_L is the Langmuir pressure, Pa; The first part on the right-hand side of Eq. (8) represents the swelling caused by a decrease in surface chemical potential energy, and the second part is the compression caused by gas pressure. The theoretical model (P&C model for short) is highly consistent with the laboratory measurement results [32], so it is widely accepted. Subsequently, this relation was extended to analyze adsorption swelling models for both multi-layer adsorptions [38] and different gas components [39].

Currently, it is considered that the adsorption swelling results from the decrease in surface chemical potential energy. However, adsorption is also an exothermic process. The heat released by gas adsorption is manifest within the coal reservoir as an increase in temperature [4–6,11] and thermal expansion. Thermal deformation results from the thermal excitation of the molecules comprising the coal [40–42]. This is different from a change in surface chemical potential energy, although the surface chemical potential energy will decrease with the increase of temperature. Previous studies have neglected this effect of temperature change on adsorption swelling. Therefore, this work analyzes and evaluates the influence of temperature change on adsorption swelling through laboratory observations and compared it with the P&C model.

3. Sample preparation and experiments

3.1. Sample preparation

Samples were collected from six coal mines: Dahuangshan (DHS), Wudong (WD), Qimei (QM), Xiaogangou (XGG), and Liuhuanggou (LHG) mines on the southern margin of the Junggar Basin, and the Tongtai (TT) mine in the Turpan Hami Basin, Xinjiang, China (Fig. 1). The coals are mainly high volatile bituminous coals with an $R_{o,max}$ between 0.34% and 0.67%. Because this paper is a general study on the thermal expansion caused by gas adsorption, there are no special requirements for the metamorphic degree ($R_{o,max}$) of the sample. Block samples were collected from a fresh working face and reduced to the target size specification of each experiment to reduce the impact of sample heterogeneity. Vitrinite reflectance and maceral contents were defined for all samples. The samples were then crushed to 60–80 mesh for isothermal adsorption experiments and heats of adsorption, crushed to 120 mesh for specific heat capacity and industrial analysis experiments. 5 mm × 20 mm cylindrical samples were prepared for the thermal expansion experiments.

3.2. Experiments

All industrial analyses were completed to an ISO17.246–2005 standard. Coal macerals and vitrinite reflectance was determined based on ISO 7404.3–1994 and ISO 7404.5–1994. This can provide basic sample characterization of coal samples.

Isothermal adsorption experiments at different temperatures were conducted based on the GB/T 19560–2008 standard. Isothermal adsorption experiments at different temperatures were carried out with ISO-300 isothermal adsorption instrument (TERRTEK, American). Firstly, 60–80 mesh samples were placed in a sealed container to measure the methane adsorbed volume in adsorption equilibrium at the same temperature and different pressure; Then, according to Langmuir monolayer adsorption theory, Langmuir volume (V_L), Langmuir pressure (P_L) and isothermal adsorption curve are obtained through

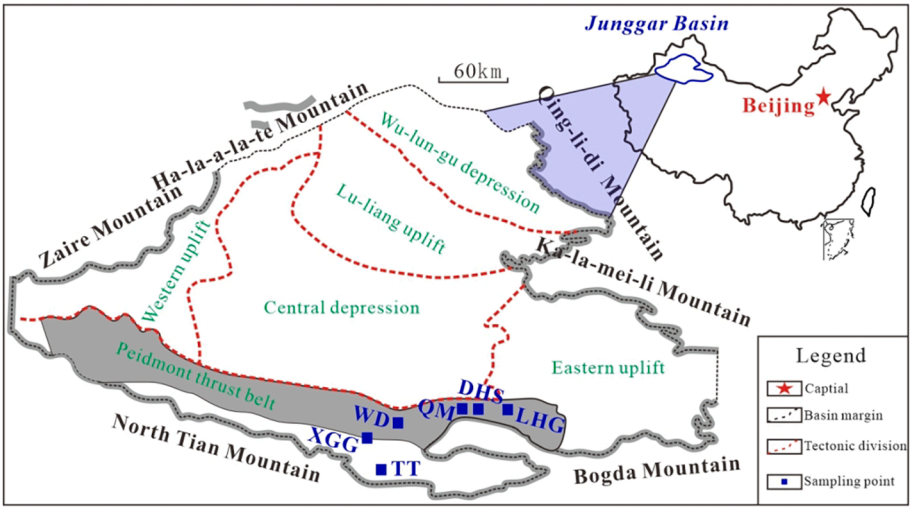

Fig. 1. Geographical location of sample collection locations.

theoretical calculation. The isothermal adsorption experimental temperatures are 30 °C, 40 °C, and 50 °C respectively. The experimental pressure is 0–15 MPa with a total of 10 pressure points, and the equilibrium time of each pressure point is 12 h. Refer to Perera et al., 2012 for detailed operation steps.

A C80 microcalorimeter (SETARAM, France) was used for the measurement of **heats of adsorption** (Fig. 2a). This microcalorimeter uses differential heat flow micro-calorimetry. Two 1.5 g coal samples were weighed and placed separately into the sample and reference cells (Fig. 2b). The sample and reference cells are surrounded by hundreds of thermocouples in linear series to record the temperature difference between the sample cell and the reference cell. The thermal difference of the sample cell and the reference cell are obtained by integrating the heat flow difference curve [17]. The temperature resolution and heat flux resolution of the C80 calorimeter is 0.01 K and 0.1μw respectively. After evacuating the cell, methane was introduced into the sample cell at a predetermined pressure. The furnace temperature, coal temperature, and heat flow parameters of the coal sample were recorded. When the heat flow curve declines to be zero, the methane cylinder is closed and the experiment ended. Experiments are at adsorption pressures of 1 MPa, 1.5 MPa, 2 MPa, and 4 MPa. The ambient temperature during the experiment was maintained at 30 °C.

Specific heat capacity was measured by DSC Q2000 (TA company, USA). First, the temperature is raised to a predetermined level and the empty crucible is placed within the sample holder and a blank baseline is measured. Then the DSC curves of standard sapphire and coal samples are determined under the same conditions. Based on the difference between the two curves, the corresponding specific heat capacity is calculated [43]. Since specific heat capacities are temperature dependent, we record specific heat capacities at 20 °C, 30 °C, 40 °C, 50 °C and 60 °C.

Thermal expansion was measured by TMA 402 F3 (NETZSCH company, Germany) (Fig. 3a). The instrument measures thermal expansion with temperature to a displacement resolution of 0.125 nm. The sample is placed on the sample support with a vertical force of 0.001 N applied to the base to fix the sample. The temperature is then raised from 30 °C to 50 °C at a rate of 5 °C/min with the equilibrium length of the sample measured while maintaining a constant fixing force of 0.001 N, the downward movement of this support records the swelling displacement/strain of the sample.

4. Results and discussion

During methane adsorption, heat release, temperature increase, and thermal expansion occur concurrently [5–8,28]. We use measured data and theoretical characterizations to define heats of adsorption from the temperature rise in coal to methane adsorption. The increment in temperature resulting from adsorption, combined with the coal thermal expansion data and comparison with the P&C model [32] defines the contribution of thermal expansion to adsorptive swelling. Finally, the difference in thermal deformation between laboratory and in-situ coal reservoir conditions and the reasons why the temperature change and thermal deformation are ignored are analyzed.

4.1. Adsorption heat characteristics

The calorimetric data enable the integral heat of adsorption characteristics of coal in methane to be defined and to then evaluate temperature change.

4.1.1. Integral heat of adsorption characteristics

Fig. 4 shows typical heat flow curves defining heat release with time as a result of methane adsorption. At any given adsorption pressure, the heat flow rate increases rapidly to a maximum and then slowly decreases to the background (Fig. 4a). This is because, in the initial stage of adsorption, the rapid adsorption of methane generates heat faster than it can be removed by conduction. Adsorption rate slows with time, as the diffusion length into the particles increases, and heat loss by conduction now outstrips heat generation [12]. The heat flow rate gradually increases with an increase in pressure and the peak value correspondingly increases (Fig. 4a). The integral heat of adsorption can be obtained for any pressure by integrating the heat flow rate [12]. In the current pressure range, the integral adsorption heat increases linearly with increasing adsorption pressure (Fig. 4b).

The integral heat of adsorption was measured for all six samples and the differential heat of adsorption was calculated from isothermal adsorption data (Table 2). The measured data show that the differential heat of adsorption of the samples was ~ 15.50–76.33 kJ/mol at an adsorption pressure of 4 MPa but mostly between 15.50 and 40 kJ/mol, with an average of 31.77 kJ/mol. The integral heat of adsorption is in the range 9.19–11.11 J/g with an average of 10.17 J/g, again at 4 MPa pressure. The maximum pressure of the calorimetry experiment is 4 MPa, and under this pressure, the coal sample is not fully saturated, so when the coal is saturated under higher pressure, the integral adsorption heat will be higher.

The integral heat of adsorption increases exponentially with increasing adsorption volume (Fig. 5a), and increases linearly with an increase in pressure (Fig. 5b). The relationship between adsorption pressure and integral heat of adsorption is similar to a Langmuir adsorption curve [12]. The linear relationship of Fig. 5a is for the maximum adsorption pressure of 4 MPa and congruent to results for lower pressures [12]. Adsorption volumes vary widely between different coals but differences in integral heats of adsorption are small. This indicates that the adsorption capacity is not a direct parameter to directly measure the adsorption heat, which will be described through theoretical analysis below.

Based on the thermodynamics of adsorption, the differential heat of adsorption is equivalent to the change in enthalpy (ΔH), expressed as [44]:

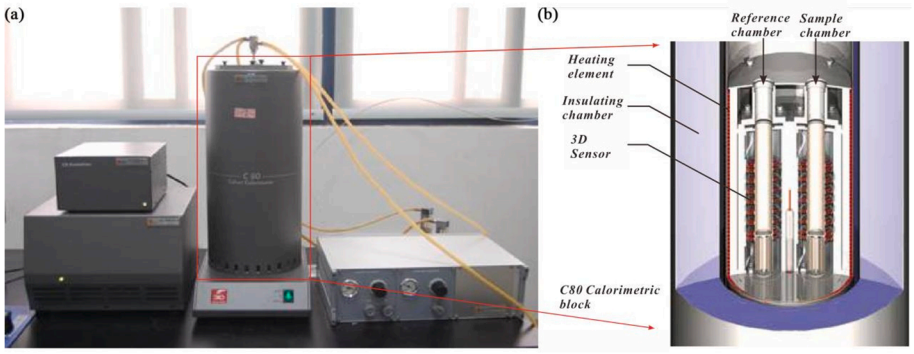

Fig. 2. C80 calorimeter. (a): Photograph identifying major components. (b): Internal structure of test tank.

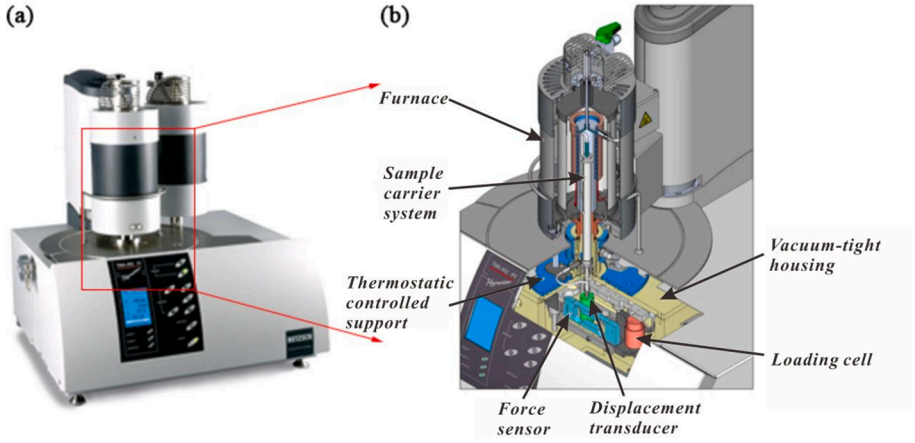

Fig. 3. Schematic diagram of TMA 402 F3. (a): instrument appearance. (b): internal structure of test tank.

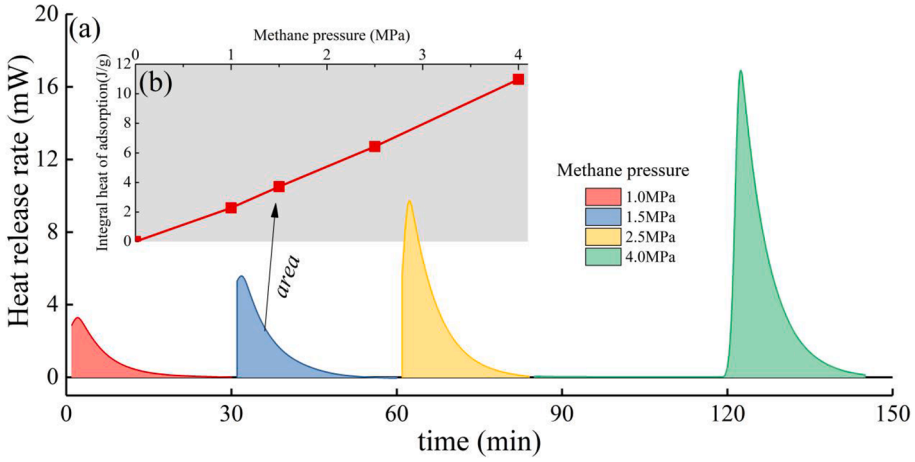

Fig. 4. Heat release rate and integral adsorption heat at different adsorption pressures. (a) relationship between heat release rate and time; (b) relationship between the integral adsorption heat and adsorption pressure.

Table 1
Industrial analyses, coal petrography and vitrinite reflectance of coal samples.

No.	M_{ad}/ %	A_d/%	V_{daf}/ %	Vitrinite/ %	Inertinite/ %	Exinite/ %	$R_{o,max}$/ %
DHS	1.46	4.12	38.08	60.80	37.49	1.71	0.62
WD	3.82	2.83	34.96	58.00	41.40	0.60	0.61
QM	1.08	12.47	47.68	93.63	1.27	5.10	0.60
XGG	0.80	10.89	34.41	35.22	63.53	1.25	0.67
LHG	1.56	4.55	23.84	6.80	92.52	0.68	0.62
TT	3.12	4.95	31.42	18.58	79.78	1.64	0.34

Table 2
Adsorption capacity, integral heat of adsorption and differential heat of adsorption at 4 MPa.

No.	V(cm^3/ g)	Q(J/ g)	Q_{st}(kJ/ mol)	No.	V(cm^3/ g)	Q(J/ g)	Q_{st}(kJ/ mol)
DHS	12.19	10.97	20.16	XGG	13.05	9.34	16.03
WD	13.05	11.11	19.08	LHG	5.77	10.41	40.44
QM	5.77	9.49	34.85	TT	3.14	10.69	76.33

$$Q_{st} = -\Delta H_{st} = R\left(\frac{\partial lnp}{\partial 1/T}\right)_V \tag{9}$$

where V is the adsorption volume (the subscript indicates that the equation is for the same adsorption amount), mol/kg; T is the temperature, K; p is the adsorption pressure, Pa. If two pressures of the adsorption isotherm (p_1 and p_2) are defined at two experimental temperatures (T_1 and T_2) at the same adsorption capacity V, then Eq. (9) can be approximately written as [45]:

$$Q_{st} = -R\left(\frac{lnp_2 - lnp_1}{1/T_2 - 1/T_1}\right)_V = RT_1T_2\left(\frac{lnp_2/p_1}{T_2 - T_1}\right) \tag{10}$$

where T_1 and T_2 are the experimental temperatures of the two isothermal adsorption experiments, K; p_1 and p_2 are the corresponding pressures under the same adsorption capacity V at T_1 and T_2, Pa. Most previous studies are based on Eq. (10) [10–11,45]. The integral heat of adsorption is then:

$$Q = Q_{st}V = VRT_1T_2\left(\frac{lnp_2/p_1}{T_2 - T_1}\right) \tag{11}$$

Isothermal adsorption data at 30 °C, 40 °C, and 50 °C were used to calculate the integral heat of adsorption (Fig. 6). Based on Eq. (11), the change in integral heats of adsorption for different adsorption amounts are obtained (Fig. 7). To meet the calculation of adsorption heat at three temperatures, different maximum adsorption capacities are selected based on different isothermal adsorption data. For example, the

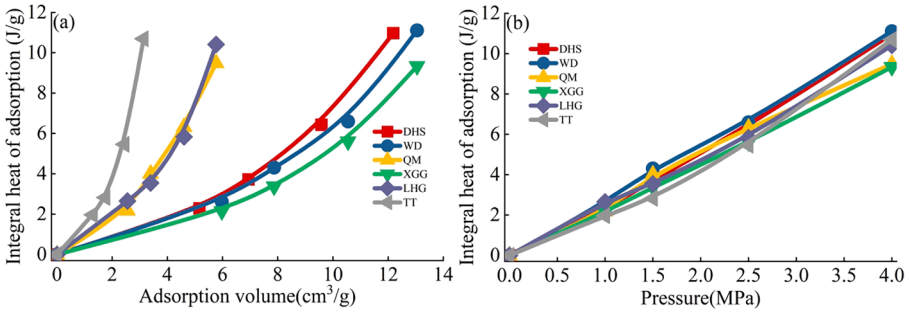

Fig. 5. Relationship between integral heat of adsorption and adsorption volume and adsorption pressure. (a) integral heat of adsorption with adsorption capacity; (b): integral heat of adsorption with adsorption pressure.

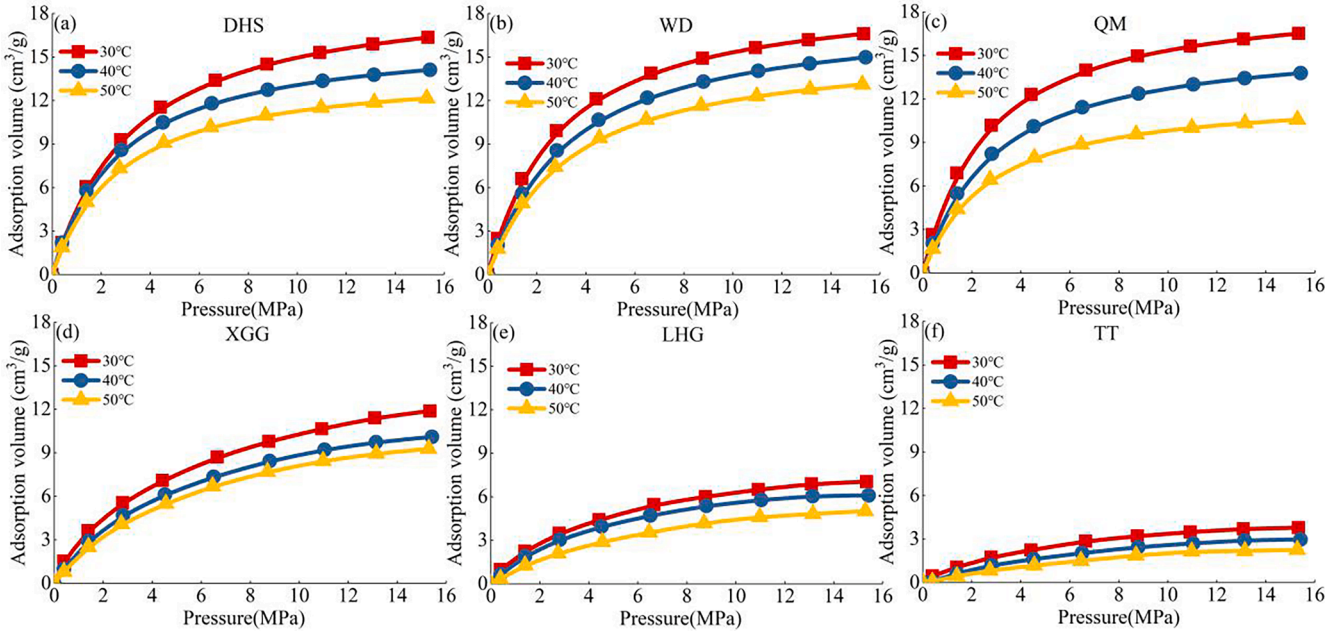

Fig. 6. Isothermal adsorption curves at 30 °C, 40 °C, and 50 °C. There are differences in isothermal adsorption capacity between different samples. Combined with the data analysis in Table 1, it can be seen that this is caused by the difference of coal metamorphic degree and vitrinite content of different samples [46–48].

adsorption capacity of DHS, WD, QM, and XGG samples is higher, so the maximum adsorption capacity of abscissa in Fig. 7 is 10 cm^3/g, while the adsorption capacity of LHG and TT samples is lower, so the maximum adsorption capacity of abscissa is 7 cm^3/g (LHG) and 3.5 cm^3/g (TT). (Fig. 7). With an increase in adsorption volume, the integral heat of adsorption increases exponentially (Fig. 7), consistent with the change observed directly from calorimetry (Fig. 5b). Comparing integral heats of adsorption measured at different temperatures, it is found that for the same temperature difference and adsorption volume, the higher the temperature, the greater the integral heat of adsorption. For measurements at the same temperature, the greater the temperature difference, the higher the integral heat of adsorption (Fig. 7). To compare the observations recovered from the calorimetry with theoretical values, the measured data are shown in Fig. 7. The calculated integral heat of adsorption at 30-40 °C is consistent with the measured magnitude with an error of less than 10%. This is because the test temperature and temperature difference between the isothermal adsorption curve of 30-40 °C is the closest of all measured data. The premise of Eq. (11) is that the adsorption volume changes small with a small temperature change [44]. Therefore, to calculate the integral heat of adsorption from thermodynamic relations, it is necessary to select an isothermal adsorption curve with a small temperature difference. This also shows that as long as the experimental temperatures of the two are close, the measured result and the theoretical calculation results are highly consistent.

4.1.2. *Variation of coal temperature during methane adsorption*

The integral heat of adsorption requires knowledge of the specific heat capacity to evaluate temperature change. Measurements at different temperatures define the specific heat capacities of our coal samples as between 0.8 and 1.6 J/g·K, with an average of 1.17 J/g·K (Table 3). Specific heat capacity increases linearly with an increase in temperature (Fig. 8), but the rate of change rate is relatively low. The difference of specific heat capacity between 20 °C and 60 °C is only ~ 0.15 J/g·K.

In the ideal isentropic (fully insulated) condition, it is assumed that all the heat released by methane adsorption on the surface of the coal matrix is absorbed by the coal matrix and the free methane in the matrix pores. That is, the absorbed heat (Q_a) is equal to the integral adsorption heat (Q):

$$Q_a = Q \tag{12}$$

The temperature change ΔT is:

$$\Delta T = \frac{Q_t}{\gamma} = \frac{Q_{st}}{\gamma_c(1-\phi_0)+\gamma_m\phi_0} \tag{13}$$

where γ_c is specific heat capacity, J/g·K; and γ_m is the specific heat

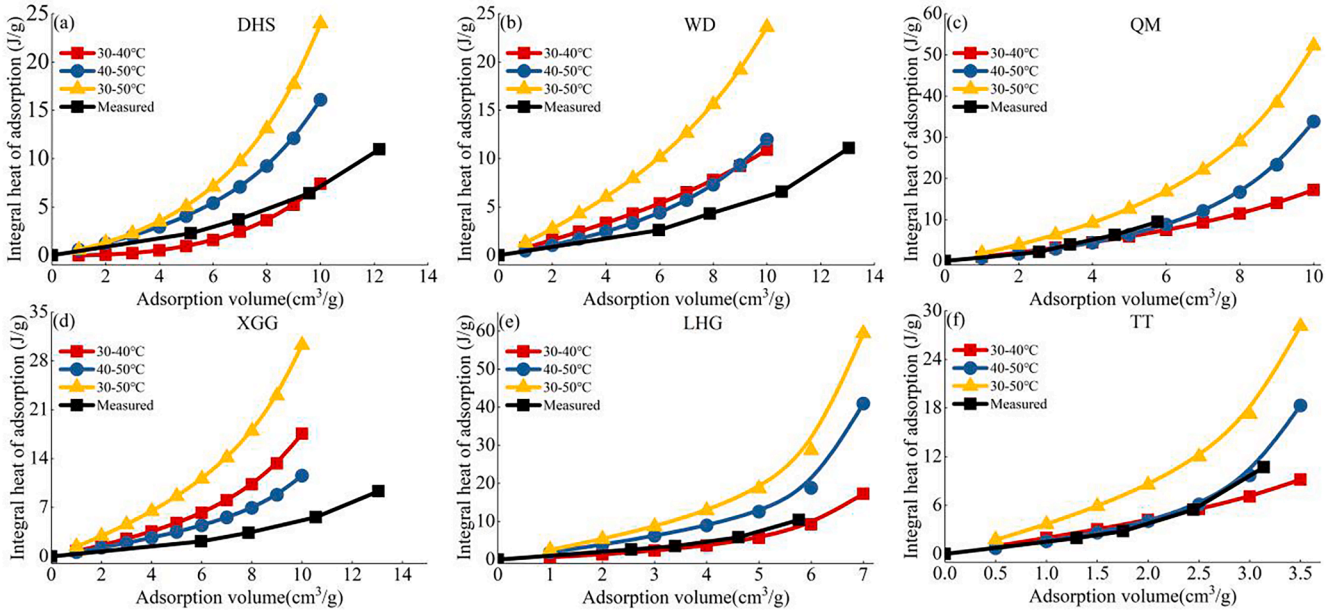

Fig. 7. Integral heat of adsorption and adsorption volume at different temperatures and over different ranges in temperature.

Table 3
Specific heat capacites of coals at different temperatures.

T	DHS	WD	QM	XGG	LHG	TT
°C	J/g·K	J/g·K	J/g·K	J/g·K	J/g·K	J/g·K
20	0.8233	1.062	0.8774	1.019	1.466	1.488
30	0.8731	1.107	0.9242	1.039	1.476	1.519
40	0.9217	1.164	0.9786	1.066	1.493	1.551
50	0.971	1.222	1.036	1.09	1.507	1.583
60	1.018	1.282	1.088	1.115	1.518	1.616
Average	0.92142	1.1674	0.98084	1.0658	1.492	1.5514

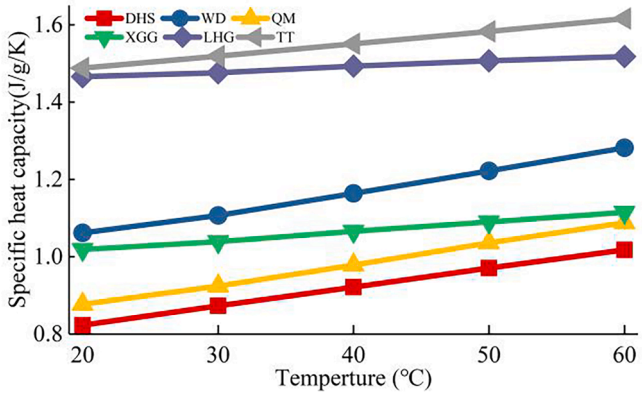

Fig. 8. Change in specific heat capacity with increasing temperature.

capacity of free methane at constant pressure, J/g·K. Because the methane is mainly adsorbed to the surface of the coal matrix, the content of free methane in the matrix pores is low and can be ignored. Therefore, Eq. (13) can be rewritten as follows:

$$\Delta T = \frac{Q_{st}}{\gamma_c} \tag{14}$$

Although the specific heat capacity changes with the temperature, the change range are small (Fig. 8). Combined with the experimental temperature and the integral adsorption heat, the temperature of coal will float at 40 °C, so the specific heat capacity measured at 40 °C is selected as the representative specific heat capacity of coal samples. According to the integral adsorption heat and isothermal adsorption data at different temperatures, the corresponding adsorption volumes at different pressures were obtained. The temperature increment increases exponentially with an increase in the adsorption volume (Fig. 9a) and linearly with pressure (Fig. 9b). This shows that during CBM production, when the reservoir pressure drops below the critical desorption pressure, the reservoir temperature will decrease linearly with a decrease in reservoir pressure [8]. When a large amount of methane is produced, the reservoir temperature will decrease exponentially.

The above calculation results assume that all the heat released by adsorption is absorbed by coal under isentropic conditions, but the heat is not likely to be fully absorbed by coal because of the presence of free and adsorbed methane. Therefore, we compared the measured data from previous research of high volatile bituminous coal [4–5,13]. The results show that the current data are consistent with the previous results in the range of temperature change (Fig. 10). Although there are differences, the hypothesis in this study is relatively reasonable. Our sample does not reach the maximum adsorption capacity at 4 MPa, indicating that the temperature increment will further increase with the continuous adsorption of methane.

4.2. Thermal expansion and its contribution to adsorption swelling in methane adsorption

An increase in temperature will result in thermal expansion [18–22,28–29]. The contribution of thermal expansion to adsorptive swelling may be determined by comparing our various data.

4.2.1. Thermal expansion/swelling characteristics of coal

The thermal strain increases linearly with increasing temperature (Fig. 11), identifying a near-constant thermal expansion coefficient. The linear thermal strain of the samples ranges from 0.03% to 0.1% over a temperature increment of 20 °C. The rate of linear thermal strain with temperature can be expressed as a coefficient of linear thermal expansion:

$$\alpha = \frac{\varepsilon}{\Delta T} \tag{15}$$

where α is the coefficient of linear thermal expansion, K^{-1}; ε is the measured linear thermal strain, defined by the change in sample length;

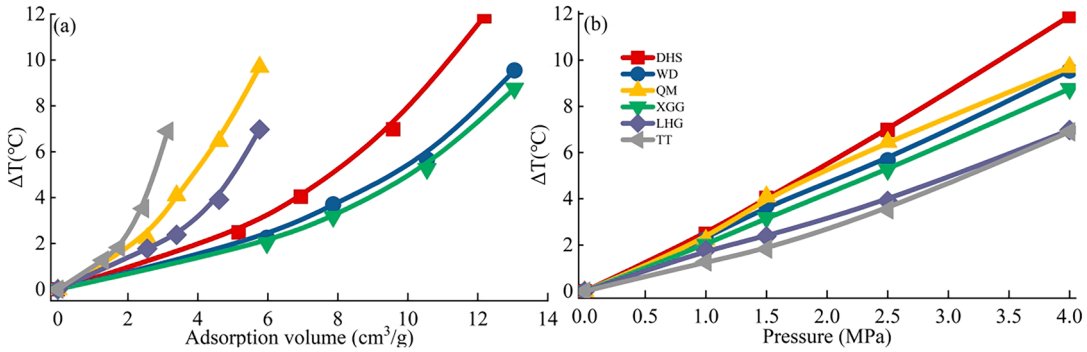

Fig. 9. Relationship between temperature increment and adsorption volume and adsorption pressure. (a): adsorption volume versus temperature increment; (b): adsorption pressure versus temperature increment.

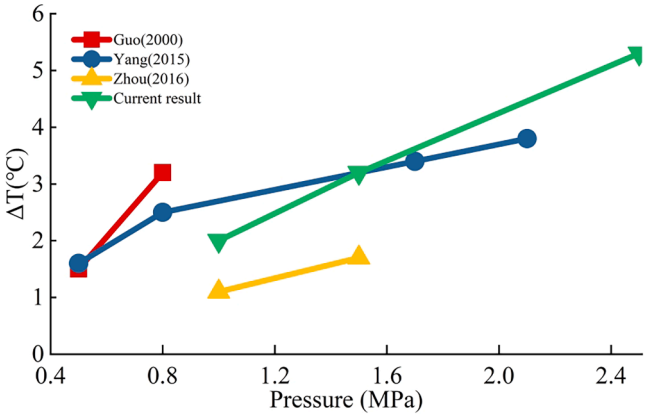

Fig. 10. comparison between the measured results of predecessors and the calculation results in this work in high volatile bituminous coal. The data of Guo (2000) [4] and Yang (2015) [13] are the internal temperature changes of the sample, while Zhou (2016) [5] is the surface of the sample, so the temperature is lower. The data in this paper are the average values of all samples.

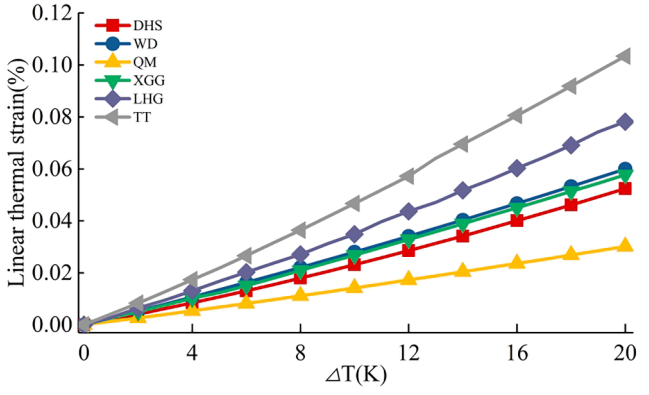

Fig. 11. Change in linear thermal expansion strain with increasing temperature.

and ΔT is a temperature difference, K. The coefficient of linear thermal expansion of the samples ranges from 0.0015%/K to 0.0052%/K, with an average of 0.0032%/K. The coefficient is different for different samples (Fig. 12a). It can be seen that the thermal expansion of the sample WD with the lowest $R_{o,max}$ is larger than that of the other five samples (Fig. 12b), which may be due to the lower strength caused by the lower metamorphic degree [49].

Combined with the temperature increase resulting from methane

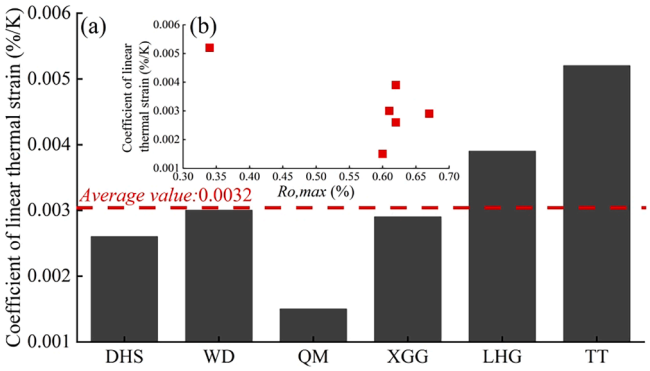

Fig. 12. Coefficients of linear thermal expansion of coal samples and their relationship with $R_{o,max}$. (a) Coefficient of linear thermal strain for different samples; (b): Coefficient of linear thermal strain with increasing $R_{o,max}$.

adsorption (Fig. 9), the overall thermal expansion caused by methane adsorption is plotted in Fig. 13. The linear strain increases exponentially with an increase in the adsorbed volume (Fig. 13a) and increases linearly with increasing pressure (Fig. 13b). This is consistent with the trend in adsorption swelling as a function of adsorption volume and pressure [25,34,50–52] (Fig. 14).

In terms of the relationship between pressure and adsorption swelling, previous experimental results show that the pressure and linear strain are similar to the Langmuir curve (Fig. 14b). At low pressure (less than4MPa), the relationship between pressure and linear strain is approximately linear, which is consistent with the current results (Fig. 13b). Previous studies [4–6,17] and current experimental data show that the heat released as a result of methane adsorption can result in the significant thermal expansion (Fig. 13), with this thermal expansion included in the adsorption swelling.

4.2.2. *Adsorption swelling model with thermal expansion*

Pan and Connell (P&C) established a widely accepted theoretical model of adsorption swelling [32] (Eqs. (7) and (8)), but this model ignores the thermal expansion caused by temperature rise. In the widely used P&M permeability model, adsorption swelling is considered to be the thermal expansion effect caused by adsorption exothermic [1]:

$$\alpha dT = \frac{d}{dP}\left(\frac{\varepsilon\beta p}{1+\beta p}\right)dp \tag{16}$$

but Palmer and Mansoori did not provide experimental data to support their view.

Laboratory and field observations indicate that reservoir temperature will rise during methane adsorption [4–7,9,53]. The swelling caused by the decline of surface chemical potential energy during

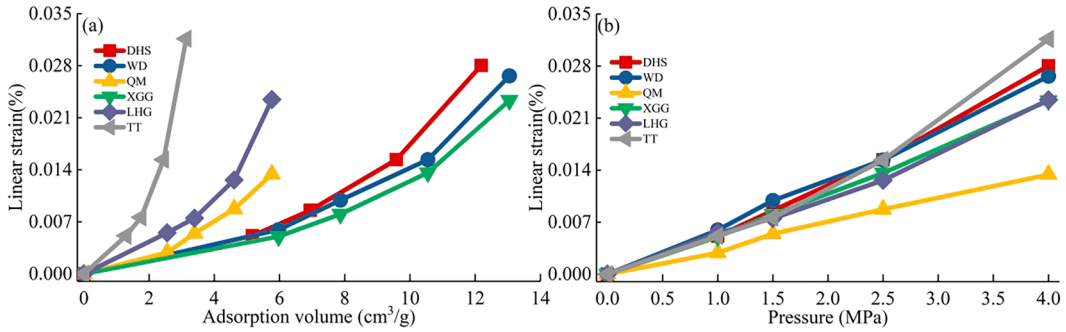

Fig. 13. Relationship between adsorption swelling based on temperature rise and adsorption volume and pressure. (a) Linear strain and adsorption volume; (b) Linear strain and pressure.

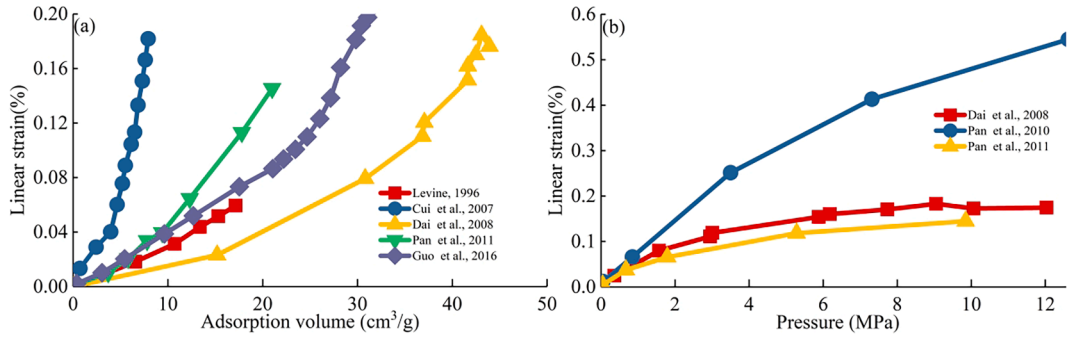

Fig. 14. Relationship between adsorption swelling with adsorption volume and pressure (Levine, 1996; Cui et al., 2007; day et al., 2008; Pan et al., 2011; Guo et al., 2016) (a) Adsorption expansion and adsorption capacity; (b): Adsorption expansion and adsorption pressure.

adsorption has also been widely discussed [30–31,35–37]. Therefore, it can be considered that adsorption swelling is the combined result of thermal expansion and the decline of surface potential energy. It is necessary to understand the relationship between the swelling caused by the decline in surface potential energy and the thermal expansion caused by temperature rise to evaluate the validity of Eqs. (8) and (16). Therefore, the integral heat of adsorption and thermal expansion data are used to determine the thermal strain resulting from methane adsorption. According to Eq. (10), two isothermal adsorption curves at different temperatures (T_0 and T) can be used to calculate the integral heat of adsorption:

$$Q = VRTT_0\frac{lnp/p_0}{T-T_0} \tag{17}$$

Based on Eq. (14), the temperature change is:

$$\Delta T = \frac{\Delta H}{\gamma} = VRTT_0\frac{lnp/p_0}{\gamma(T-T_0)} \tag{18}$$

and the swelling caused by the exothermic heat liberated by methane adsorption is:

$$\varepsilon = \Delta T\alpha = VRTT_0\frac{\alpha ln(p/p_0)}{\gamma(T-T_0)} \tag{19}$$

Based on the first part of Eq. (8), Eq. (19), and the data in Table. 4, the thermal expansion resulting from the temperature rise and the swelling based on surface potential energy change are calculated. The trend of expansion in the two models with adsorption volume and pressure are completely consistent (Fig. 15), and also consistent with the measured swelling (Fig. 14). Comparing the two models, the swelling caused by the decline in surface potential energy is greater than that caused by the temperature rise (Fig. 15). Based on results for the six samples, the thermal strain is approximately 57% of that due to the change in surface potential energy, that is, the thermal strain of the samples accounts for ~ 35% in average of the total strain during methane adsorption (Fig. 15a-e) – although the thermal expansion disappears as temperature equilibrate. Indeed, the thermal strain of one sample accounts for ~ 50% of the total strain (Fig. 15f). This indicates that although the swelling caused by the decline in surface potential energy is the main factor for adsorption swelling, the thermal expansion caused by exothermic effects cannot be ignored. This also indicates that

Table 4
Parameters required for adsorption swelling calculations.

No.	T K	T_0 K	V_L m³/t	P_L MPa	α %	γ J/g·K	E_s MPa	v_s	ρ_s g/cm³	φ	$f(x,v_s)$
DHS	313	303	16.48	2.57	0.0026	0.922	5386	0.23	1.44	0.05	0.77
WD	313	303	17.99	3.10	0.0030	1.164	4590	0.26	1.28	0.05	0.74
QM	313	303	16.23	2.73	0.0015	0.977	4787	0.25	1.45	0.04	0.75
XGG	313	303	13.66	5.42	0.0029	1.066	3220	0.24	1.41	0.06	0.76
LHG	313	303	8.08	4.60	0.0039	1.493	3852	0.23	1.39	0.09	0.77
TT	313	303	4.78	8.71	0.0052	1.551	2132	0.27	1.37	0.11	0.74

Note: Porosity (φ) is calculated based on true density and apparent density. The Young's modulus (E_s) and Poisson's ratio (v_s) of skeleton were calculated based on uniaxial compression experiment with constant axial displacement rate of 0.1 mm/min and formula 5.

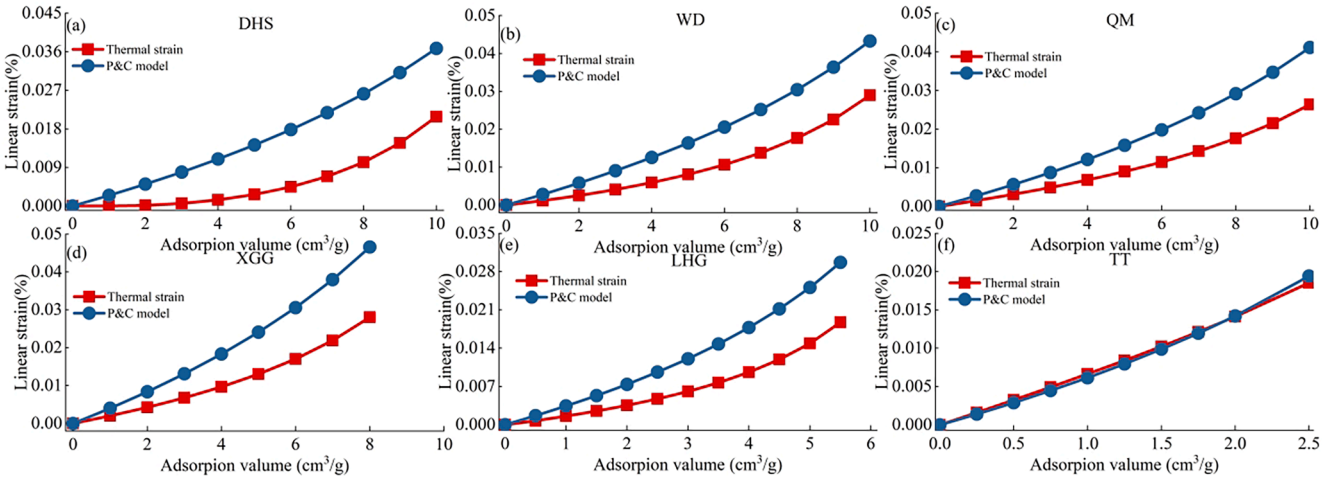

Fig. 15. Change in linear strain with increasing adsorption volume based on P-C and thermal expansion models.

the assumption of the P&M model, that the adsorptive strain contributes 100% to the thermal strain, and that the P&C model considers that the swelling is purely due to the decline in surface potential energy, are not completely accurate.

By summing the contributions of Eqs. (8) and (19), the adsorption swelling at low pressure is obtained as:

$$\varepsilon = RTV_L ln\left(1+\frac{p}{p_0}\right)\frac{\rho_s}{E_s}f(x,v_s) + VRTT_0\frac{\alpha ln(p/p_0)}{\gamma(T-T_0)} - \frac{p}{E_s}(1-2v_s) \quad (20)$$

Adsorption swelling calculated based on Eq. (20) showed that the trend in the change in strain with increasing pressure is consistent with the shape of the Langmuir adsorption curve (Fig. 16) [54]. Fig. 16 shows results for three samples (DHS, WD, and QM). The other three samples (XGG, LHG, and TT) exhibit negative swelling (net shrinkage) based on Eq. (20), indicating that the compression due to the incremented gas pressure is always greater than the swelling caused by adsorption. This is because the Langmuir volume of the three samples is very small, while the Langmuir pressure is very high (Table 4). This results in a lower surface potential energy and reduced temperature changes in the adsorption process, resulting in the combined effects of swelling being less than the compression caused by gas pressure.

4.2.3. Analysis of thermal expansion during laboratory and in-situ coal reservoir conditions

The thermal expansion of coal caused by temperature increase will decrease with the conductive loss of heat and cooling. This is different from the swelling caused by the change of chemical potential energy resulting from adsorption. It is worth noting that adsorption swelling experiments in the laboratory should reset strains rapidly with cooling, but this is not observed (Fig. 17B-d) [2,50,55]. This is because the smaller sample size and slower absorption rate in the laboratory make the heat difficult to preserve (Fig. 17A-a), resulting in thermal expansion which is difficult to measure due to the fast temperature drop (Fig. 17B-a). But in the in-situ coal reservoir, the temperature changes can be preserved for a longer time than that in the laboratory due to the lower heat dissipation [8,9,56,57].

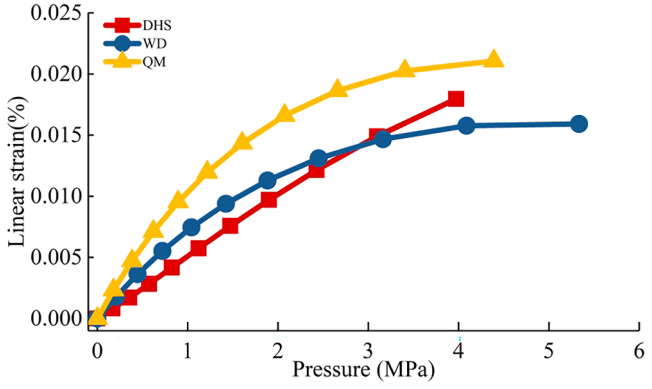

Fig. 16. Evolution of linear strain with increasing pressure, based on Eq. (15). Eq. (15) comprises three parts: 1) swelling caused by a decline in surface potential energy; 2) thermal expansion caused by heat release as a result of adsorption; and 3) compression caused by gas pressure.

Most of the samples used in adsorption deformation experiments are cylinders or cubes smaller than ~ 25 mm in size [50,51,55]. Such a small sample is not conducive to heat preservation [6,7]. Moreover, the adsorption rate of bulk samples is much lower than that of powder samples, and the adsorption equilibrium time under a given pressure exceeds 48 hrs [50,55], which leads to a lower exothermic rate. Especially, as adsorption equilibrium is approached, the adsorption rate is very low [55]. Since the ambient temperature in the laboratory is near-constant (Fig. 17a-a), thus the strain at adsorption equilibrium will not include thermal expansion strain (Fig. 17b–d). The experimental results of Zhou (2017) [6] and Feng (2017) [7] show that at a pressure of 1.5 MPa, the surface temperature of the coal sample will rise to the maximum value of 1 °C in 20 s, and then begin to decrease and decrease by 80% after 150 s - indicating that heat loss is rapid. The results of Guo (2000) show that at an adsorption pressure of 0.7 MPa, then a temperature sensor inside the sample indicates a temperature increase of 3.4 °C after 1 hr and this decreased by 30% in the following 3 hrs [4]. Yang and Nie (2015) also show that the internal heat loss of the sample is slower than that of the surface [13]. But compared with the adsorption equilibrium time of tens of hours [50,55] the gain in heat is near fully lost during the progress to adsorption equilibrium. Therefore, the measured adsorption strain at each pressure point only includes the strain caused by the change of surface chemical potential (Fig. 17b-c), which is why the P&C theoretical model, neglecting the adsorption thermal expansion well matches the experimental data [32].

But thermal expansion effects will be retained longer in larger in-situ coal reservoirs (Fig. 16a-b). For a large length scale of conduction and low thermal conductivity of ~ 0.2WW/(m·k) of the coal reservoir [8], the temperature change of the reservoir will be retained longer than in the laboratory. Fan (2019) used numerical simulation techniques to study the production process of coalbed methane under the condition of an in-situ reservoir [8], the results show that in the absence of external fluid injection, the desorption of methane leads to a continuous decline in reservoir temperature, while with the injection of carbon dioxide, adsorption and heat release lead to an increase of 18 °C in the reservoir temperature, which continues to maintain [8]. This is because the larger

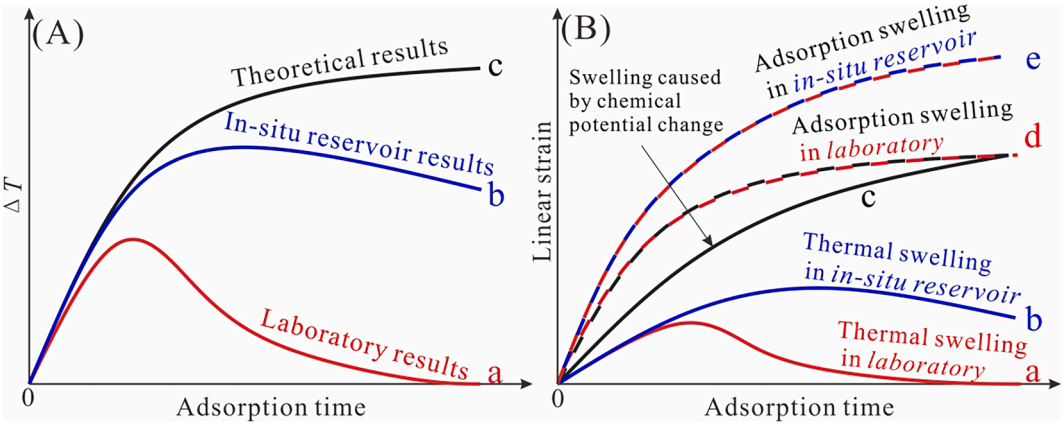

Fig. 17. The temperature and strain change with adsorption time under laboratory and in-situ reservoir conditions. (A): temperature change versus adsorption time. Where (a) is the result of laboratory measurement. Due to the rapid heat dissipation, the increase of temperature is lower than that of heat dissipation, and the temperature decreases gradually until it is the same as the test environment temperature; Where (b) is the temperature changes in the in-situ reservoir. Due to the larger reservoir size and sealing conditions, the heat loss is slower and the temperature change can keep a slow change. Where (c) is the theoretical temperature change. Therefore, under the same pressure, the adsorption capacity gradually decreases, and the heat release also decreases, and finally reaches the adsorption equilibrium. The heat release is positively correlated with the adsorption capacity, so under the same pressure, with the adsorption process, the adsorption rate gradually decreases, the heat release rate also decreases, and finally reaches the adsorption equilibrium. (B): Strain versus adsorption time. Where (a) is the thermal expansion strain in the laboratory adsorption swelling. Due to the loss of heat, the thermal strain gradually decreases and disappears. Where (b) is thermal expansion strain under the in-situ reservoir. The thermal strain can be maintained due to low heat dissipation; Where (c) is the strain caused by the decrease of surface chemical potential during adsorption, which is the main part of adsorption strain; Where (d) is the adsorption strain measured in the laboratory, which is the sum of the strain of *curve a* and *curve c*; Where (e) is the adsorption strain under in-situ condition, which is the sum of the strain of *curve b* and *curve c*.

length scale and heat dissipation of the in-situ reservoir limit the rate of temperature reduction [8]. This phenomenon is also more apparent in the process of gas outburst with rapid methane desorption [9,57]. In the early stage and during the occurrence of gas outbursts, methane desorption makes the reservoir temperature decrease rapidly [9,56–59]. Due to the low thermal conductivity of the reservoir and the rapid nature of the outburst event, the temperature change can be maintained throughout the process (Fig. 17a-b). Therefore, temperature change within the reservoir can be used as a precursor to predicting gas outbursts [4,56,57]. In the CBM production [59] and the CGS [3], the coal deformation and permeability change caused by temperature change in methane desorption and carbon dioxide adsorption is also worthy of attention.

5. Conclusions

The heat of adsorption and temperature change due to methane adsorption in six high volatile coals are analyzed based on calorimetry and concepts of thermodynamics. Thermal expansion measurements link the contribution of thermal expansion to methane adsorption and adsorption swelling. Conclusions are as follows:

1) The integral heat of adsorption increases exponentially with an increase in gas adsorption volume and increases logarithmically with increasing adsorption pressure. The thermal strain increases exponentially with adsorption volume and increases logarithmically with pressure. These observations are consistent with the variation of adsorption swelling with adsorption volume and pressure measured directly in the laboratory.
2) Adsorption swelling in coal is a combination of the swelling caused by the decline in surface potential energy and temperature increase, rather than either in isolation. In ideal isentropic conditions, swelling caused by the decline in surface potential energy dominates, followed by that due to temperature rise, accounting for approximately 35% in average of the total strain presented by methane adsorption – but dissipating depending on the insulating conditions.
3) Laboratory experiments of adsorption swelling under non-isentropic (isothermal) conditions, the thermal expansion in the adsorption process cannot be accurately measured due to the rapid heat loss - this thermal expansion is therefore not measured. However, in the in-situ environment of a coalbed reservoir, the lower heat dissipation capacity will retain this deformation for a longer period and thereby impact permeability.

Declaration of Competing Interest

The authors declare that they have no known competing financial interests or personal relationships that could have appeared to influence the work reported in this paper.

Acknowledgments

This work was supported by the National Natural Science Foundation of China (41772158, 52174139) and the development of large oil and gas fields and CBM in major national scientific and technological projects (2016ZX05043-004-001).

References

[1] Palmer I, Mansoori J. How permeability depends on stress and pore pressure in coalbeds: a new model. In SPE annual technical conference and exhibition. Society of Petroleum Engineers. 1996. https://doi.org/10.2118/36737-MS.
[2] Z. Pan, L.D. Connell, Modelling of anisotropic coal swelling and its impact on permeability behaviour for primary and enhanced coalbed methane recovery, Int. J. Coal Geol. 85 (3-4) (2011) 257–267, https://doi.org/10.1016/j.coal.2010.12.003.
[3] K. Wang, J. Pan, E. Wang, Q. Hou, Y. Yang, X. Wang, Potential impact of CO_2 injection into coal matrix in molecular terms, Chem. Eng. J. 401 (2020) 126071, https://doi.org/10.1016/j.cej.2020.126071.
[4] L.W. Guo, Q.X. Yu, K. Wang, Experimental study on change in coal temperature during adsorbing gas, J China Univ Min Technol 29 (2000) 287–289.
[5] Zhou D, Feng ZC, Zhao D, Zhao YS Cai TT. Uniformity of temperature variation in coal during methane adsorption. J Nat Gas Sci Eng 2016; 33: 954-960. https://doi.org/10.1016/j.jngse.2016.06.010.
[6] D. Zhou, Z.C. Feng, D. Zhao, Y.S. Zhao, T. Cai, Experimental meso scale study on the distribution and evolution of methane adsorption in coal, Appl. Therm. Eng. 112 (2017) 942–951, https://doi.org/10.1016/j.applthermaleng.2016.10.164.
[7] Z.C. Feng, T.T. Cai, D. Zhou, D. Zhao, Y.S. Zhao, C. Wang, Temperature and deformation changes in anthracite coal after methane adsorption, Fuel 192 (2017) 27–34, https://doi.org/10.1016/j.fuel.2016.12.005.

[8] C.J. Fan, D. Elsworth, S. Li, Z.W. Chen, M.K. Luo, Y. Song, H.H. Zhang, Modelling and optimization of enhanced coalbed methane recovery using CO_2/N_2 mixtures, Fuel 253 (2019) 1114–1129, https://doi.org/10.1016/j.fuel.2019.04.158.

[9] B. Zhou, J. Xu, S. Peng, J. Geng, F. Yan, Test system for the visualization of dynamic disasters and its application to coal and gas outburst, Int. J. Rock Mech. Min. 122 (2019) 104083, https://doi.org/10.1016/j.ijrmms.2019.104083.

[10] G. Yue, Z. Wang, X.u. Tang, H. Li, C.e. Xie, Physical simulation of temperature influence on methane sorption and kinetics in coal (II): temperature evolvement during methane adsorption in coal measurement and modeling, Energy Fuels 29 (10) (2015) 6355–6362, https://doi.org/10.1021/acs.energyfuels.5b01637.

[11] A. Nodzeński, Sorption and desorption of gases (CH_4, CO_2) on hard coal and active carbon at elevated pressures, Fuel 77 (11) (1998) 1243–1246, https://doi.org/10.1016/S0016-2361(98)00022-2.

[12] J.H. Kang, D. Zhang, F.B. Zhou, H.J. Li, T.Q. Xia, Numerical modeling and experimental validation of fractional heat transfer induced by gas adsorption in heterogeneous coal matrix, Int. J. Heat Mass Trans. 128 (2019) 492–503, https://doi.org/10.1016/j.ijheatmasstransfer.2018.08.087.

[13] T. Yang, B.S. Nie, Temperature variation tests during the gas adsorption process, J. China Coal Soc. 40 (2015) 380–385.

[14] J.K. Liu, C.X. Wang, X.Q. He, S.H. Li, Infrared measurement of temperature field in coal gas desorption, Int. J. Min. Sci. Technol. 2014 (24) (2014) 57–61, https://doi.org/10.1016/j.ijmst.2013.12.010.

[15] Z.X. Liu, Z.C. Feng, Q.M. Zhang, D. Zhao, H.Q. Guo, Heat and deformation effects of coal during adsorption and desorption of carbon dioxide, J. Nat. Gas Sci. Eng. 25 (2015) 242–252, https://doi.org/10.1016/j.jngse.2015.04.024.

[16] D. Zhao, H. Chen, J. An, D. Zhou, Z. Feng, Distribution law of temperature changes during methane adsorption and desorption in coal using infrared thermography technology, AIP Adv. 8 (5) (2018) 055325, https://doi.org/10.1063/1.5029432.

[17] H.J. Li, J.H. Kang, F.B. Zhou, Z.Y. Qiang, G.H. Li, Adsorption heat features of coalbed methane based on microcalorimeter, J. Loss Prevent Proc. 55 (2018) 437–449, https://doi.org/10.1016/j.jlp.2018.05.006.

[18] M. Wierzbicki, B. Dutka, The influence of temperature changes of the structurally deformed coal-methane system on the total methane content, Arch. Min. Sci. 55 (2010) 547–560.

[19] J. Sobczyk, A comparison of the influence of adsorbed gases on gas stresses leading to coal and gas outburst, Fuel 115 (2014) 288–294, https://doi.org/10.1016/j.fuel.2013.07.016.

[20] D.H. Bangham, R.E. Franklin, Thermal expansion of coals and carbonised coals, Trans. Faraday Soc. 42 (1946) B289–B294.

[21] J.C. Macrae, C. Ryder, RyderC. Thermal expansion of coal, 265, Nature 176 (4475) (1955) 265, https://doi.org/10.1038/176265a0.

[22] W.C. Zhu, C.H. Wei, J. Liu, H.Y. Qu, D. Elsworth, A model of coal–gas interaction under variable temperatures, Int. J. Coal Geol. 86 (2-3) (2011) 213–221, https://doi.org/10.1016/j.coal.2011.01.011.

[23] L.D. Connell, M. Lu, Z. Pan, An analytical coal permeability model for tri-axial strain and stress conditions, Int. J. Coal Geol. 84 (2) (2010) 103–114, https://doi.org/10.1016/j.coal.2010.08.011.

[24] Z.W. Chen, J.S. Liu, Z.J. Pan, L.D. Connell, D. Elsworth, Influence of the effective stress coefficient and sorption-induced strain on the evolution of coal permeability: model development and analysis, Int. J. Greenh Gas Con. 8 (2012) 101–110, https://doi.org/10.1016/j.ijggc.2012.01.015.

[25] X.J. Cui, R.M. Bustin, L. Chikatamarla, Adsorption-induced coal swelling and stress: implications for methane production and acid gas sequestration into coal seams, J. Geophys. Res. Sol Ea 112 (2007) B10202, https://doi.org/10.1029/2004JB003482.

[26] T. Nakagawa, I. Komaki, M. Sakawa, K. Nishikawa, Small angle X-ray scattering study on change of fractal property of Witbank coal with heat treatment, Fuel 79 (11) (2000) 1341–1346, https://doi.org/10.1016/S0016-2361(99)00269-0.

[27] Y.D. Cai, D.M. Liu, Y.B. Yao, Z.T. Li, Z.J. Pan, Partial coal pyrolysis and its implication to enhance coalbed methane recovery, Part I: an experimental investigation, Fuel 132 (2014) 12–19, https://doi.org/10.1016/j.fuel.2014.04.084.

[28] Z.Q. Li, X.F. Xian, Q.M. Long, Experiment study of coal permeability under different temperature and stress, J. China Univ. Min. Technol. 38 (2009) 523–527.

[29] Y.Q. Hu, Y.S. Zhao, D. Yang, Z.Q. Kang, Experiment study of effect of temperature on permeability characteristics of lignite, Chin. J. Rock Mech. Eng. 29 (2010) 1585–1590.

[30] Yates DJC. The expansion of porous glass on the adsorption of non-polar gases. Proceedings of the Royal Society of London. Series A. Math Phys Sci 1954; 224: 526-544.

[31] G.W. Scherer, Dilatation of porous glass, J. Am. Ceram. Soc. 69 (6) (1986) 473–480, https://doi.org/10.1111/j.1151-2916.1986.tb07448.x.

[32] Z. Pan, L.D. Connell, A theoretical model for gas adsorption-induced coal swelling, Int. J. Coal Geol. 69 (4) (2007) 243–252, https://doi.org/10.1016/j.coal.2006.04.006.

[33] Z.J. Pan, L.D. Connell, Modelling permeability for coal reservoirs: a review of analytical models and testing data, Int. J. Coal Geol. 92 (2012) 1–44, https://doi.org/10.1016/j.coal.2011.12.009.

[34] J.R. Levine, Model study of the influence of matrix shrinkage on absolute permeability of coal bed reservoirs, Geol. Soc. Lond. Spec. Publ. 109 (1) (1996) 197–212, https://doi.org/10.1144/GSL.SP.1996.109.01.14.

[35] Bangham DH, Fakhoury N. The swelling of charcoal. Part I.—Preliminary experiments with water vapour, carbon dioxide, ammonia, and sulphur dioxide. Proceedings of the Royal Society of London. Series A, Containing Papers of a Mathematical and Physical Character 1930; 130: 81-89. https://doi.org/10.1098/rspa.1930.0189.

[36] Bangham, DH, Fakhoury N, Mohamed AF. The swelling of charcoal. Part III. Experiments with the lower alcohols. Proceedings of the Royal Society of London. Series A-Math Phys Sci 1934; 147: 152-175. https://doi.org/10.1098/rspa.1934.0212.

[37] Bangham DH. The swelling and shrinkage of porous materials and the role of surface forces in determining technical strength. In Symposium Society Chemical Industry 1946.

[38] Z. Pan, Modeling of coal swelling induced by water vapor adsorption, Front. Chem. Sci. Eng. 6 (1) (2012) 94–103, https://doi.org/10.1007/s11705-011-1172-2.

[39] C.R. Clarkson, Z.J. Pan, I.D. Palmer, S. Harpalani, Predicting sorption-induced strain and permeability increase with depletion for coalbed-methane reservoirs, SPE J. 15 (2010) 152–159, https://doi.org/10.2118/114778-PA.

[40] Z. Feng, Y. Zhao, Z. Wan, Experiment study of the thermal deformation of in-situ gas coal, in: M. Cai (Ed.), Rock Mechanics: Achievements and Ambitions, CRC Press, 2011, pp. 103–108, https://doi.org/10.1201/b11438-22.

[41] S. Ghabezloo, Effect of porosity on the thermal expansion coefficient of porous materials, in: In Poromechanics V: Proceedings of the Fifth Biot Conference on Poromechanics, 2013, pp. 1857–1866, https://doi.org/10.1061/9780784412992.220.

[42] C. Wang, J. Feng, J. Liu, M. Wei, C. Wang, B. Gong, Gong BDirect observation of coal–gas interactions under thermal and mechanical loadings, Int. J. Coal Geol. 131 (2014) 274–287, https://doi.org/10.1016/j.coal.2014.06.021.

[43] F. Hanrot, D. Ablitzer, J.L. Houzelot, M. Dirand, Experimental measurement of the true specific heat capacity of coal and semicoke during carbonization, Fuel 73 (2) (1994) 305–309, https://doi.org/10.1016/0016-2361(94)90130-9.

[44] A.L. Myers, Thermodynamics of adsorption in porous materials, AIChE J. 48 (1) (2002) 145–160, https://doi.org/10.1002/aic.690480115.

[45] M. Bülow, D. Shen, S. Jale, Measurement of sorption equilibria under isosteric conditions: the principles, advantages and limitations, Appl. Surf. Sci. 196 (1-4) (2002) 157–172, https://doi.org/10.1016/S0169-4332(02)00052-1.

[46] M. Mastalerz, W. Solano-Acosta, A. Schimmelmann, A. Drobniak, Effects of coal storage in air on physical and chemical properties of coal and on gas adsorption, Int. J. Coal Geol. 79 (4) (2009) 167–174, https://doi.org/10.1016/j.coal.2009.07.001.

[47] M.S.A. Perera, P.G. Ranjith, S.K. Choi, D. Airey, P. Weniger, Estimation of gas adsorption capacity in coal: a review and an analytical study, Int. J. Coal Prep Util. 32 (1) (2012) 25–55, https://doi.org/10.1080/19392699.2011.614298.

[48] S. Tao, S.D. Chen, D.Z. Tang, X. Zhao, H. Xu, S. Li, Material composition, pore structure and adsorption capacity of low-rank coals around the first coalification jump: a case of eastern Junggar Basin, China, Fuel 211 (2018) 804–815, https://doi.org/10.1016/j.fuel.2017.09.087.

[49] H.O. Balan, F. Gumrah, Assessment of shrinkage-swelling influences in coal seams using rank-dependent physical coal properties, Int. J. Coal Geol. 77 (1-2) (2009) 203–213, https://doi.org/10.1016/j.coal.2008.09.014.

[50] S. Day, R. Fry, R. Sakurovs, Swelling of Australian coals in supercritical CO_2, Int. J. Coal Geol. 74 (1) (2008) 41–52, https://doi.org/10.1016/j.coal.2007.09.006.

[51] Z.J. Pan, L.D. Connell, M. Camilleri, Laboratory characterization of coal reservoir permeability for primary and enhanced coalbed methane recovery, Int. J. Coal Geol. 82 (2010) 252–261, https://doi.org/10.1016/j.coal.2009.10.019.

[52] X. Guo, Z.M. Wang, Y.L. Zhao, A comprehensive model for the prediction of coal swelling induced by methane and carbon dioxide adsorption, J. Nat. Gas Sci. Eng. 36 (2016) 563–572, https://doi.org/10.1016/j.jngse.2016.10.052.

[53] J. Liu, C. Wang, X. He, S. Li, Infrared measurement of temperature field in coal gas desorption, J. China Univ. Min. Technol. 24 (1) (2014) 57–61.

[54] D.H. Moffat, K.E. Weale, Sorption by coal of methane at high pressures, Fuel 34 (1955) 449–462.

[55] B. Zhang, X. Fu, Z.e. Deng, Y. Shen, M. Hao, A comparative study on the deformation of unconfined coal during the processes of methane desorption with successively decreasing outlet pressure and with constant outlet pressure, J. Petrol. Sci. Eng. 195 (2020) 107531, https://doi.org/10.1016/j.petrol.2020.107531.

[56] H.T. Wang, X.F. Xian, J.M. He, Y.C. Lv, R.S. Ji, J.G. Zhang, Inquisition of forecasting dangerousness of heading face outburst by drillings and coalbed temperature indices, J. Chongqing Univ. (Nat. Sci. Ed.) 22 (1999) 36–40.

[57] B.S. Nie, Y.K. Ma, S.T. Hu, J.Q. Meng, Laboratory study phenomenon of coal and gas outburst based on a mid-scale simulation system, Sci. Rep. 9 (2019) 1–12, https://doi.org/10.1038/s41598-019-51243-4.

[58] M. Gawor, J. Rysz, Visualisation of coal desintegration and investigation of rapid changes of gas pressure, temperature and strain during gas-geomechanical phenomena, Arch. Min. Sci. 47 (2002) 3–22.

[59] Y. Li, Z. Wang, S. Tang, D. Elsworth, Re-evaluating adsorbed and free methane content in coal and its ad-and desorption processes analysis, Chem. Eng. J. 428 (2022) 131946, https://doi.org/10.1016/j.cej.2021.131946.